RESEARCH ARTICLE | SEPTEMBER 12 2017

Influence of the particle size on polarization-based rangegated imaging in turbid media

Heng Tian; Jingping Zhu [0]; Shuwen Tan; Yunyao Zhang; Xun Hou



AIP Advances 7, 095310 (2017) https://doi.org/10.1063/1.4995576





Articles You May Be Interested In

Polarimetry in turbid, birefringent, optically active media: A Monte Carlo study of Mueller matrix decomposition in the backscattering geometry

J. Appl. Phys. (May 2009)

Third-order scattering model for the diffuse backscattering intensity patterns of polarized light from a turbid medium

Appl. Phys. Lett. (April 2007)

New approach for absolute fluence distribution calculations in Monte Carlo simulations of light propagation in turbid media

J. Appl. Phys. (February 2014)







Influence of the particle size on polarization-based range-gated imaging in turbid media

Heng Tian, Jingping Zhu, a Shuwen Tan, Yunyao Zhang, and Xun Hou Key Laboratory for Physical Electronics and Devices of the Ministry of Education and Shaanxi Key Lab of Information Photonic Technique, Xi'an Jiaotong University, Xi'an 710049, China

(Received 12 July 2017; accepted 4 September 2017; published online 12 September 2017)

The influence of size of the scatterer on the image contrast for polarization-based range-gated imaging in turbid media is investigated here by Monte Carlo method. Circularly polarized light would be more efficient to eliminate the noise photons for both the isotropic medium as well as the anisotropic medium, as compared with linearly polarized light. The improvement in contrast is pronounced for isotropic medium using either linear or circular polarization. The plausible explanations for these observations are also presented. © 2017 Author(s). All article content, except where otherwise noted, is licensed under a Creative Commons Attribution (CC BY) license (http://creativecommons.org/licenses/by/4.0/). [http://dx.doi.org/10.1063/1.4995576]

I. INTRODUCTION

Improving the visibility of target buried in turbid media using optical techniques is a challenging problem. Polarization imaging techniques, ¹⁻⁶ due to the relative simplicity of instrumentation, have been extensively used to enhance the viewing visibility. The factor that limits the effectiveness of those methods is the polarimetric difference between the light being scattered from the target and that from the turbid media. Thus, it is of significant importance to understand how the polarization characteristic influenced by the state of polarization of the incident light, the target type and the morphological parameters of the medium such as size, concentration, and refractive index. Several investigations have been conducted in the past to analyze the relations between the polarization properties of the scattered light and the parameters of the turbid media and the target. Hielscher et al. observed that the spatial intensity distribution of the backscattered light depends on the optical parameters. Zimnyakov et al. revealed that the influence of the anisotropy parameters of the turbid media on the propagation of the incident light. 8 Ghosh et al.'s preceding work showed that the refractive index of a scatterer affects the depolarization of the incident light. Yiaohui Ni and Alfano reported on the effect of the particle size on the state of polarization of the backscattered light for linear and circular polarization. In turbid medium composed of larger scattering particles, for polarization gating imaging, circularly polarized light could improve the image contrast as compared with linearly polarized light. Nothdurft and Gang Yao demonstrated that the scattering coefficient, absorption coefficient and anisotropy parameter of the turbid medium affect the polarization image. 11 They also indicated that polarization detection could be used to discriminate material type. 12 A study on impact of optical properties of the turbid media to the photon pathlength was performed by Xinxin Guo et al. 13 The study that the scattering and absorption coefficients have an effect on the polarization characteristics of the forward-scattered light was performed by Cochenour et al. 14 When the polarized light propagates in finite sample, Ghatrehsamani and Town reported that how the boundaries of the turbid media modify the polarization state of the scattered light. 15 The effect of the dynamics of the particles on the propagation of light was investigated by Singh et al. 16 They demonstrated by simulations and experiments that the phase fluctuation carried by light propagating throughout the scattering environment with the external drive has a nonzero mean under



^aElectronic mail: jpzhu@xjtu.edu.cn

suitable circumstances. The existence of fluctuation may affect the polarization state of the light beam.

Additionally, the influence of optical properties on the polarization state at a single scattering event has also been investigated. Laan *et al.*¹⁷ performed simulations for the evolution of polarization state after 1, 2, and 10 scattering events in various scattering environments comprising particles of different sizes. Kim *et al.*¹⁸ showed that the helicity of the circularly polarized photons is preserved after one forward-scattering event caused by large-sized particles. The effect of the refractive index of the particle on the polarization state of circularly polarized light at each scattering event was investigated by Min Xu *et al.*¹⁹ Xinxin Guo *et al.*²⁰ concluded that the surviving polarization fraction of circularly polarized light is larger than that of linearly polarized light after a single scattering event in the forward-scattering medium.

These studies clearly show that the variations in optical properties of the turbid media and the target affect the effectiveness of polarization imaging techniques. It might be beneficial to utilize the implications of these results for the applications of polarization imaging in turbid media.

Polarization-based range-gated technology (PR), combining polarization difference imaging and range-gated technology, was implemented to further improve the image quality in scattering environment. It incorporates the superiority of the polarization imaging into the tail-gating technology to suppress background photons. As mentioned above, having a better understanding of an imaging method is essential for optical imaging applications. Therefore, in order to understand the effective imaging method properly, it is rather nontrivial to investigate the effects of the optical properties of the turbid medium on the target detection of polarization-based range-gated technology in detail. In this work, we have investigated the effects of the particle size on polarization-based range-gated technology through Monte Carlo method. The image quality for linearly and circularly polarized incident light has been also investigated.

II. MONTE CARLO SIMULATION DESCRIPTION

In this section, we implement the Stokes-Mueller formalism²² in the algorithm developed by Wang and Jacques²³ to describe the main steps of the Monte Carlo simulation for PR. Neglecting only the absolute phase, the Stokes vector that can describe the polarization state of an optical beam in terms of intensity is expressed as^{22,24}

$$\mathbf{S} = \begin{bmatrix} I \\ Q \\ U \\ V \end{bmatrix} = \begin{bmatrix} E_{\parallel} E_{\parallel}^* + E_{\perp} E_{\perp}^* \\ E_{\parallel} E_{\parallel}^* - E_{\perp} E_{\perp}^* \\ E_{\parallel} E_{\perp}^* + E_{\perp} E_{\parallel}^* \\ i(E_{\parallel} E_{\perp}^* - E_{\perp} E_{\parallel}^*) \end{bmatrix}, \tag{1}$$

where $E_{\parallel}e_{\parallel}$ and $E_{\perp}e_{\perp}$ represent the parallel and perpendicular electric fields in the plane perpendicular to the propagation direction u and the asterisk denotes the complex conjugate. I is the total intensity of the light beam. Q describes the amount of the linear horizontal or vertical polarization, U describes the amount of linear +45° or -45° polarization, and V describes the amount of right or left circular polarization of the light beam. The interaction of an incident polarized beam with an optical component or a propagation event is characterized by a 4 × 4 Mueller matrix \mathbf{M} . The relation can be written as

$$\mathbf{S}_{out} = \mathbf{M} \cdot \mathbf{S}_{in}. \tag{2}$$

Here S_{in} is the Stokes vector of the incident beam and S_{out} is the Stokes vector of the emerging beam.

A. Launch

A semi-infinite turbid medium, modeled as a suspension of uniformly monodispersed polystyrene microspheres in water, has a slab structure was used in the simulation. The refractive index of the scattering particles (n_p) was 1.59 and that of the surrounding medium (n_m) was 1.33. The study was carried out in two separate cases for two microsphere diameters: (1) 0.11 μ m and (2) 2 μ m.

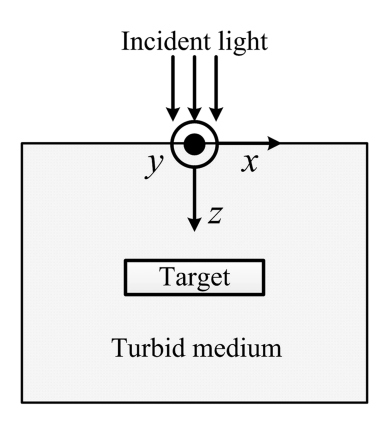


FIG. 1. The coordinate system for the Monte Carlo method.

The corresponding anisotropy parameters (g) were 0.092 and 0.914 at the incident wavelength of 632.8 nm. The scattering coefficient (μ_s) could be calculated from Mie theory. The absorption coefficient (μ_a) was set to 0.05 cm⁻¹.

A laboratory coordinate system (x, y, z) was defined as in Fig. 1. A flat light beam of 0.56 cm in diameter was injected orthogonally into the turbid medium. The perpendicular electric field vector \mathbf{e}_{\perp} and the parallel electric field vector \mathbf{e}_{\parallel} were set along x- and y-axes, respectively. The photon propagation direction \mathbf{u} was set along z-axis. Thus, \mathbf{e}_{\perp} (1, 0, 0), \mathbf{e}_{\parallel} (0, 1, 0), and \mathbf{u} (0, 0, 1) construct the initial local coordinate frame utilized to express the initial Stoke vector of the incident light beam. The initial polarization state of $\begin{bmatrix} 1 & 1 & 0 & 0 \end{bmatrix}^T$ represents linear horizontally polarized light and the initial polarization state of $\begin{bmatrix} 1 & 0 & 0 & 1 \end{bmatrix}^T$ represents right circularly polarized light.

B. Scattering

During the propagation process in the medium, a photon moves a step size s that is given based on Ref. 23. The time taken by the step size is calculated from $t = s \cdot n_m/c$. The photon weight (w) needs to be updated due to absorption of the medium. After reaching the end of the step, the photon would be scattered by a particle.

Since the Stokes vector is defined in the local coordinate frame $(e_{\perp}, e_{\parallel}, u)$, the frame must be modified to keep track of the polarization state of the photon upon each scattering event.^{27,28} The azimuthal angle ϕ and the scattering angle θ are used to describe the rotation of the electric field vectors $(e_{\perp} \text{ and } e_{\parallel})$ and of the propagation direction u respectively. As shown in Fig. 2, after each single scattering event, the electric field vectors $(e_{\perp} \text{ and } e_{\parallel})$ are rotated about the propagation direction u by the azimuthal angle ϕ firstly. The new electric field vectors $(e'_{\perp} \text{ and } e'_{\parallel})$ are determined by the matrix $\mathbf{R}(\mathbf{k}, \delta)$.²⁹ This rotation is called the azimuthal rotation. We project the Stokes vector \mathbf{S}_s given in the local coordinate frame $(e_{\perp}, e_{\parallel}, u)$ into the frame $(e'_{\perp}, e'_{\parallel}, u)$ after the azimuthal rotation. The conversion of the Stokes vector could be achieved by premultiplication of the Mueller matrix for rotation $\mathbf{R}(\phi)$ that is expressed as²²

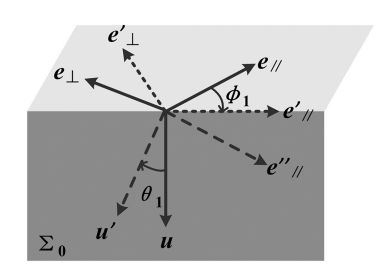


FIG. 2. The local frame rotation for the scattering.

$$\mathbf{R}(\phi) = \begin{bmatrix} 1 & 0 & 0 & 0 \\ 0 & \cos 2\phi & \sin 2\phi & 0 \\ 0 & -\sin 2\phi & \cos 2\phi & 0 \\ 0 & 0 & 0 & 1 \end{bmatrix}.$$
 (3)

The value of the azimuthal angle ϕ_1 is determined by the rejection method.^{30,31} Thus, the Stokes vector after the azimuthal rotation \mathbf{S}_{rota} is expressed as

$$\mathbf{S}_{rota} = \mathbf{R}(\phi_1) \cdot \mathbf{S}_s. \tag{4}$$

Next, the photon propagation direction is updated. In the new scattering plane Σ_0 spanned by e'_{\parallel} and u, the frame $(e'_{\perp}, e'_{\parallel}, u)$ is rotated about the perpendicular electric field vector e'_{\perp} by the scattering angle θ . The new propagation direction u' is obtained by $\mathbf{R}(\mathbf{k}, \delta)^{29}$ and the new parallel electric field vector e''_{\parallel} is obtained by cross-product $(e''_{\parallel} = u' \times e'_{\perp})$. This rotation is denoted as the scattering rotation. After the scattering rotation, we have to project the Stokes vector given in the frame $(e'_{\perp}, e'_{\parallel}, u)$ into the frame $(e'_{\perp}, e''_{\parallel}, u')$. The alteration of the Stokes vector could be obtained by premultiplication of the single scattering Mueller matrix $\mathbf{M}_S(\theta)$. Because the turbid medium is considered as composed of homogeneous microspheres and the particle size is comparable with the incident wavelength, the matrix can be derived from Mie theory, 24,25 which is written as 24

$$\mathbf{M}_{S}(\theta) = \begin{bmatrix} m_{11}(\theta) & m_{12}(\theta) & 0 & 0\\ m_{12}(\theta) & m_{11}(\theta) & 0 & 0\\ 0 & 0 & m_{33}(\theta) & m_{34}(\theta)\\ 0 & 0 & -m_{34}(\theta) & m_{33}(\theta) \end{bmatrix}.$$
 (5)

The elements of the matrix are expressed as²⁴

$$m_{11}(\theta) = \frac{1}{2} \left[|S_2(\theta)|^2 + |S_1(\theta)|^2 \right]$$

$$m_{12}(\theta) = \frac{1}{2} \left[|S_2(\theta)|^2 - |S_1(\theta)|^2 \right]$$

$$m_{33}(\theta) = \frac{1}{2} \left[S_1(\theta) S_2^*(\theta) + S_2(\theta) S_1^*(\theta) \right]$$

$$m_{34}(\theta) = \frac{i}{2} \left[S_1(\theta) S_2^*(\theta) - S_2(\theta) S_1^*(\theta) \right]$$
(6)

Here $S_1(\theta)$ and $S_2(\theta)$ depend upon the particle size, the refraction index of the particle, the Riccati-Bessel functions, the spherical Bessel functions, and the spherical Henkel functions.²⁹ In our Monte Carlo program, we used the source code by Bohren and Huffman²⁴ to determine $S_1(\theta)$ and $S_2(\theta)$.

The value of the scattering angle θ_1 can be also calculated by the rejection method.^{30,31} Thus, the Stokes vector after the scattering rotation \mathbf{S}_{scatt} is expressed as

$$\mathbf{S}_{scatt} = \mathbf{M}_{S}(\theta_{1}) \cdot \mathbf{S}_{rota},\tag{7}$$

Substituting Eq. (4) into Eq. (7), the evolution of the Stokes vector after a single scattering event is written as

$$\mathbf{S}_{scatt} = \mathbf{M}_{S}(\theta_{1}) \cdot \mathbf{R}(\phi_{1}) \cdot \mathbf{S}_{s}, \tag{8}$$

C. Collision

A reflective parallelepiped with a size of $0.2 \times 0.2 \times 0.1$ cm³ in x-, y- and z-axes located at 3.5 cm below the top surface of the medium was used as a target with the refractive index of 1.51. When the incident photons collide with the target, they are completely reflected from the target surface according to the laws of reflection. The reflection is expressed by the Mueller Matrix for reflection

 \mathbf{M}_R . According to the Fresnel laws with respect to the incident angle α_1 and the transmitted angle α_2 calculated by Snell's law, \mathbf{M}_R can be written as²²

$$\mathbf{M}_{R} = \frac{1}{2} \left(\frac{tan\alpha_{-}}{tan\alpha_{+}} \right)^{2} \begin{bmatrix} a^{2} + b^{2} & a^{2} - b^{2} & 0 & 0 \\ a^{2} - b^{2} & a^{2} + b^{2} & 0 & 0 \\ 0 & 0 & -2ab & 0 \\ 0 & 0 & 0 & -2ab \end{bmatrix},$$
(9)

where $a = cos\alpha_-$, $b = cos\alpha_+$ and $\alpha_{\pm} = \alpha_1 \pm \alpha_2$.

As illustrated in Fig. 3, in order to guarantee the validity of the Fresnel laws, the local coordinate frame has to be rotated by ϕ_2 to make e'_{\parallel} enter the incidence plane Σ_1 spanned by the photon direction u and the normal unit vector n pointing from the medium to the target firstly. At this point, e'_{\perp} is perpendicular to the incident plane. Thus, the Stokes vector must be updated by premultiplication of the Mueller matrix for rotation $\mathbf{R}(\phi_2)$. Consequently, the Stokes vector \mathbf{S}_{ref} of the photon reflected at the target surface is given as

$$\mathbf{S}_{ref} = \mathbf{M}_R \cdot \mathbf{R}(\phi_2) \cdot \mathbf{S}_r,\tag{10}$$

where S_r represents the Stokes vector before the interface collision.

It is necessary to update the local coordinate frame for the next propagation. Using the laws of reflection, the new photon direction u' can be determined. Note that the perpendicular electric field vector e'_{\parallel} is maintained during the reflection, thus the new parallel electric field vector e''_{\parallel} is obtained by cross-product $(e''_{\parallel} = u' \times e'_{\perp})$. e'_{\perp} , e''_{\parallel} and u' form the new local coordinate frame.

D. Detection

During propagation in the scattering medium, when a photon reaches the top surface of the medium, it should be detected. The Stokes vector of the emission photon is calculated in a way that simulates the actual measurement in the laboratory. The local coordinate frame of a photon is rotated by an angle ϕ_3 so that e'_{\parallel} is in the plane \sum_2 spanned by the orientation of polarizer P_{\parallel} and the normal n (see Fig. 4). Details of the operation have been presented in Ref. 32. Thus, the final Stokes vector \mathbf{S}_{final} measured by the detector is obtained by

$$\mathbf{S}_{final} = \mathbf{R}(\phi) \cdot \mathbf{S}_f. \tag{11}$$

Here S_f represents the Stokes vector before being recorded.

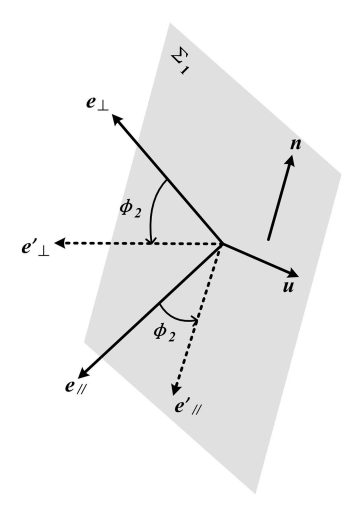


FIG. 3. The local frame rotation in the medium-target interface.

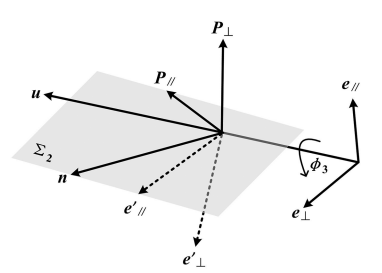


FIG. 4. The local frame rotation for the detection. P_{\parallel} and P_{\perp} are the orthogonal orientations of a polarizer, n represents the normal of the polarizer. e_{\perp} and e_{\parallel} are the perpendicular and parallel electric field vectors before the rotation operation. e'_{\perp} and e'_{\parallel} are the new perpendicular and the parallel electric field vectors after the rotation operation.

We set the time threshold value relying on the physical thickness (the distance between the top surface of the medium and the location of the target). If entire time accumulation of the propagation is greater than the time threshold value, the Stokes parameters of the photon should be recorded. According to this and using the Stokes parameters, polarization-based range-gated technology could be realized. During the entire propagation process, the Stokes vector and the direction vectors must be unitized after each operation. If the photon weight is sufficiently less than the threshold or the photon reaches the detecting plane, a new photon is launched until all the photons have been launched.²³

III. RESULTS AND DISCUSSION

In the simulations, 5×10^7 photons were launched because of the overall consideration of timeliness and reliability of the simulation results. The each simulation result was recorded with a grid of 300×300 pixels and presented as a two-dimensional image with 20×20 mm in size.

Figure 5 shows the simulation results of the target in the medium prepared using $0.11~\mu m$ diameter polystyrene microspheres with the optical thickness τ of 2.75 (the product of the scattering coefficient and the physical thickness). The intensity image is shown in Fig. 5(a) and the image obtained by polarization-based range-gated technology using linearly polarized photons (linear PR) is displayed in Fig. 5(b). The images are normalized to unity respectively. In the intensity image, the background is almost as bright as the target so that the target signal is quite weak. On the contrary, the background illumination is substantially lower than the light reflected from the target in the linear PR image. As stated above, the target is invisible in the intensity image while it is clearly visible in the linear PR image.

Image contrast, calculated using $(I_{max} - I_{min})/(I_{max} + I_{min})$, provides a quantitative method to evaluate the image quality. Here I_{max} is the average intensity of the target center area in the image and I_{min} is the average background intensity of the four equivalent areas across the four sides outside

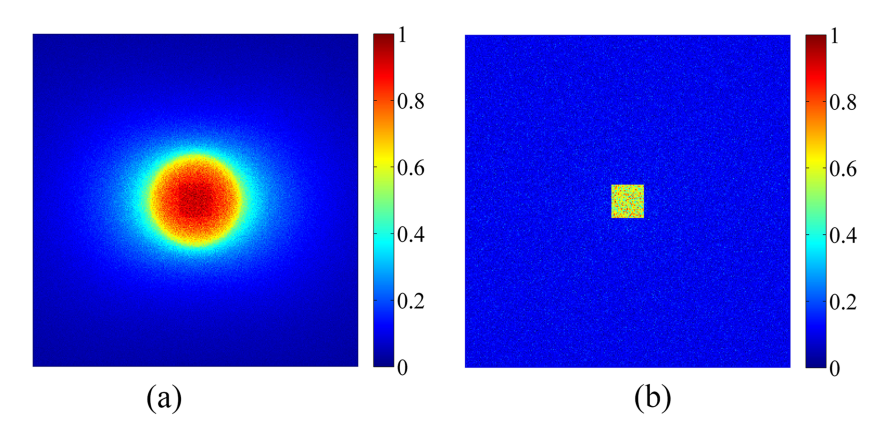


FIG. 5. The intensity image (a) and the linear PR image (b) in the medium consist of polystyrene microspheres with diameter of 0.11 μ m.

the target. Note that, by this definition, the higher the value of image contrast is, the better the image quality is. In Fig. 6, we show the image contrast versus the optical thickness obtained from isotropic medium. The optical thickness is varied by changing the scattering coefficient. Comparing the contrast curves, it can be concluded that the contrast for intensity imaging is inferior to that obtained by linear PR for all values of optical thickness. The results fully indicate that the incorporation of the polarization information into the time distribution of the photons could significantly improve the image contrast.

The effectiveness of the improvement method depends on the propagation of photon. It is known that after being incident into the turbid medium, the polarized photons can be simplified as three types according to their scattering events. Ballistic photons follow ballistic paths and have not been scattered by particles in the turbid medium. Snake photons only undergo a limited number of scattering while diffusive photons undergo multiple scattering in the medium during their propagation process.

If a target is embedded in the turbid medium, the photons may interact with the target and then carry the target information during a random step. Therefore, the photons can be classified into six categories: medium ballistic photons (MB), medium snake photons (MS) and medium diffusive photons (MD), target ballistic photons (TB), target snake photons (TS) and target diffusive photons (TD). MB, MS and MD are photons only scattered by particles. The backscattering behaviors, including single large-angle scattering and series of small-angle scattering events, make these photons back to the detection plane before reaching the target surface. They are divided into backscattered photons and act as background photons. TB, TS and TD propagate along the direction of incident photons and then along a return path after being reflected at the target surface. These photons are not affected by the backscattering behaviors. There are two main mechanisms responsible for depolarization of the photons in the scattering medium.³³ One originates from the randomization of the plane of polarization of the scattered photon. The other originates from the differences in the phase and the amplitude of two transverse electric field components as a function of scattering angle.³⁴ After a single scattering event, both the plane of polarization and the scattering angle are altered. Thus, the polarization state of the photons should be updated upon each scattering event. The cumulative alteration causes the photons encountering different scattering events having different polarization state. Note that the six kinds of photons undergo different scattering behaviors. Consequently, they carry different polarization information respectively. There are also differences in their propagation time according to their optical paths. Polarization-based range-gated technology takes full advantage of the differences in the propagation time and the polarization information to filter out noise photons and improve the image contrast.

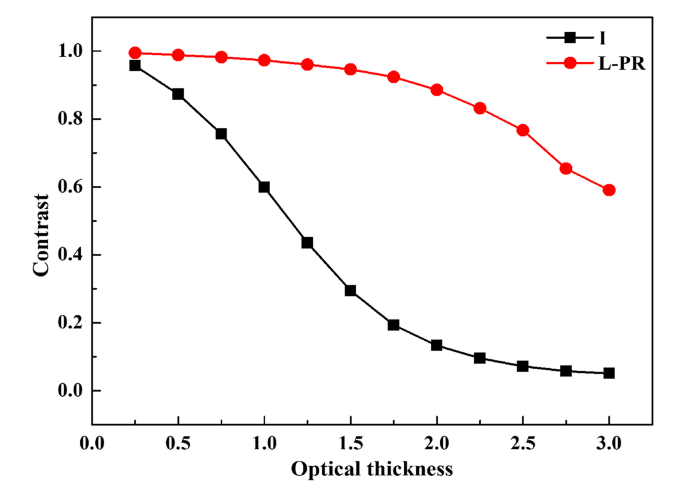


FIG. 6. Image contrast versus the optical thickness for large-sized polystyrene microspheres (g = 0.092). I: the intensity image, L-PR: the linear PR image.

We have recorded the images obtained by polarization-based range-gated technology using circularly polarized photons (circular PR) for both small-sized as well as large-sized scatterers and made comparison with the images obtained by linear PR. The contrast plot for linear and circular PR in the turbid medium containing 0.11 µm diameter polystyrene spheres is displayed in Fig. 7(a). The image quality is better for circular PR as compared to that of linear PR. A possible detailed explanation is presented here. In Fig. 7(b), we show the measured distribution of the degree of polarization (DoP) of backscattered photons with the operation of range-gated technology through the isotropic scattering medium have a value of $\mu_s = 0.714 \text{ cm}^{-1}$. For the case of linear PR, DoP is calculated by $\frac{\sqrt{Q^2 + U^2}}{I}$ and DoP is calculated by $\frac{|V|}{I}$ for the case of circular PR. ²⁴ It can be seen that the DoP of the backscattered photons is lower for circular polarization than for linear polarization after the operation of range-gated technology in the incident photon area (the range between the 110th pixel and the 190th pixel). In the isotropic medium, the backscattered photons are mainly caused by the scattering at a large angle. The helicity of circularly polarized photon is reversed after a single large-angle scattering event. 17 The helicity of the photon encountering a series of scattering events is determined by the even or odd number of spin flips in its path. 19 Since the number of scattering for each photon during the propagation process is random, the helicities of the backscattered photons are different. Due to the accumulation of the helicity, the circularly backscattered photons depolarize rapidly after multiple scattering. Consequently, circular PR could eliminate a large number of noise photons by means of polarization difference imaging method. It may be noted that range-gated technology can filter out the same amount of backscattered photons in linear and circular PR because the propagation time is independent of the state of polarization of the incident light. Therefore, circular PR could filter out

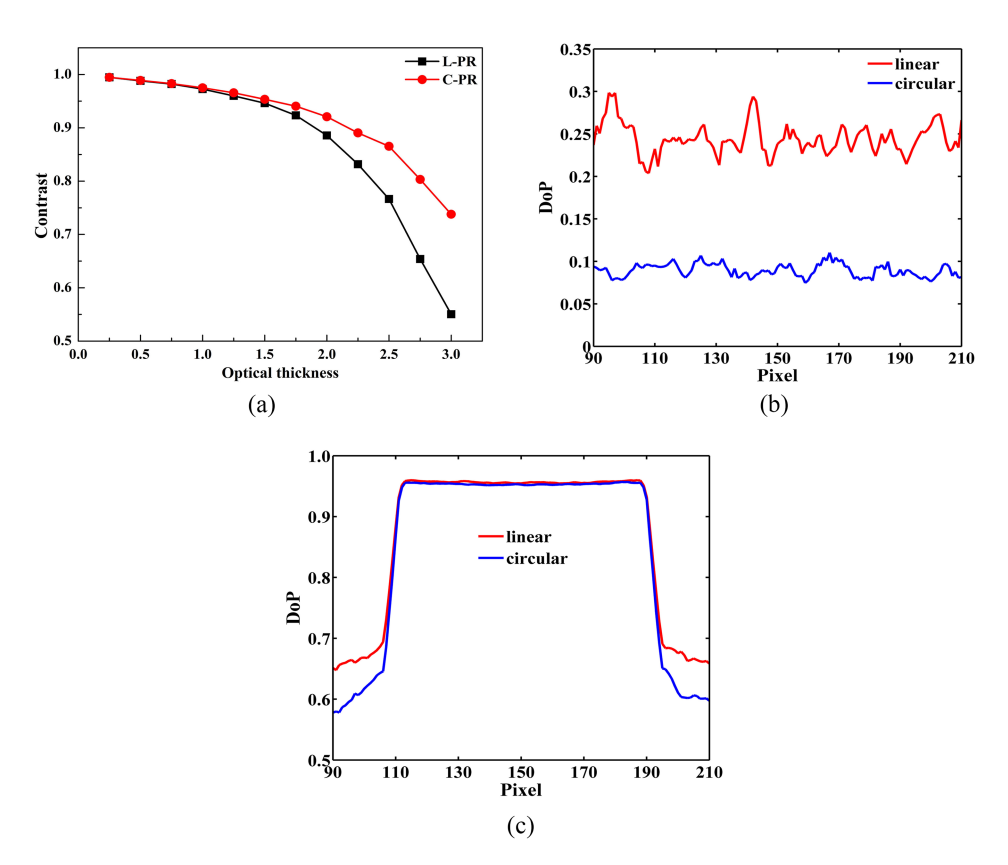


FIG. 7. (a) Variation of image contrast with the optical thickness for scattering medium containing 0.11 μ m polystyrene microspheres in diameter. L-PR: the linear PR image and C-PR: the circular PR image. (b) The spatial distribution of DoP of the backscattered photons with the operation of range-gated technology in the isotropic medium having a value of $\mu_s = 0.714 \text{ cm}^{-1}$, (c) the spatial distribution of DoP of the forward-scattered photons without target embedded in the isotropic medium having a value of $\tau = 2.5$ using linearly and circularly polarized photons.

more backscattered photons, as compared with linear PR. Furthermore, it is TB and TS that carry the target information. There is no appreciable difference in their number for the linearly and circularly polarized incident photons due to the forward-scattered photons (the photons to illuminate the target), maintaining their initial states of polarization in the two cases in the incident photon area, as shown in Fig. 7(c). These results indicate that the same amount of effective photons is recorded by linear and circular PR. The end result is that the image contrast is significantly pronounced for the case of circular polarization.

Figure 8(a) illustrates the variation in image contrast, as a function of the value of optical thickness for linear and circular PR for the turbid medium containing 2 μ m diameter polystyrene spheres. Under low optical thickness conditions, the contrast of linear PR image is equivalent to that of circular PR image. However, with the number of the scattering events increasing, the contrast is better for circular PR than for linear PR. A convenient approach for investigating this trend is to measure DoP of forward-scattered photons for the flat beam without target embedded in the anisotropic medium. We show, in Fig. 8(b), the spatial distribution of DoP of the forward-scattered photons along the horizontal direction. DoP of the forward-scattered photons for linear polarization and that for circular polarization are almost equal in the incident photon area. This is consistent with the previous report at lower value of optical thickness. The amount of TB and TS which carry the target information are recorded for linear polarization is the same as that for circular polarization in this case. In addition, the relative number of backscattered photons is so small that the almost equal amount of backscattered photons are filtered out by polarization-based range-gated technology no matter what the state of polarization of the incident photons is. As a result, the image contrast of circular PR is equivalent to that of linear PR.

Better image contrast for circular polarization could be understood on the basis that with increasing value of the scattering event, the linearly forward-scattered photons depolarize sharply as compared with the circularly forward-scattered photons owing to the circular polarization memory effect. PR is larger than that obtained by linear PR. Further, although it has been reported that DoP of the backscattered photons for circularly polarized photons is higher than that for linearly polarized photons, a displayed in Fig. 9(a), Fig. 9(b) shows that DoP has the similar distribution after the operation of the range-gated technology. This behavior is manifested by the fact that MS undergoing multiple scattering show the dominant influence on DoP, with weakly scattered photons being suppressed by the range-gated technology. According to this, the almost same amount of the backscattered photons is filtered out by PR either using linearly or circularly polarized photons. Consequently, the improvement of image contrast would be more efficient using circular PR in the medium composed of large-sized polystyrene microspheres.

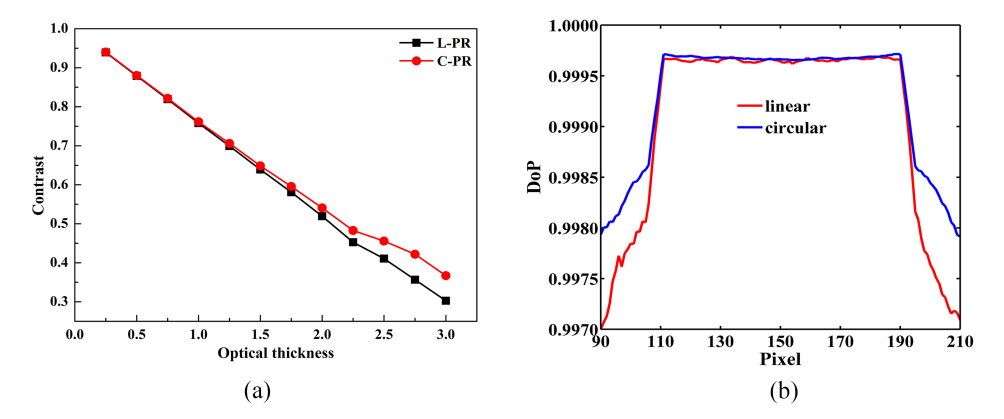


FIG. 8. (a) Variation of image contrast with the optical thickness obtained from scattering medium comprising 2 μ m polystyrene microspheres in diameter. L-PR: the linear PR image and C-PR: the circular PR image. (b) The spatial distribution of DoP of the forward-scattered photons without target embedded in the anisotropic medium having a value of $\tau = 0.75$ using linearly and circularly polarized photons.

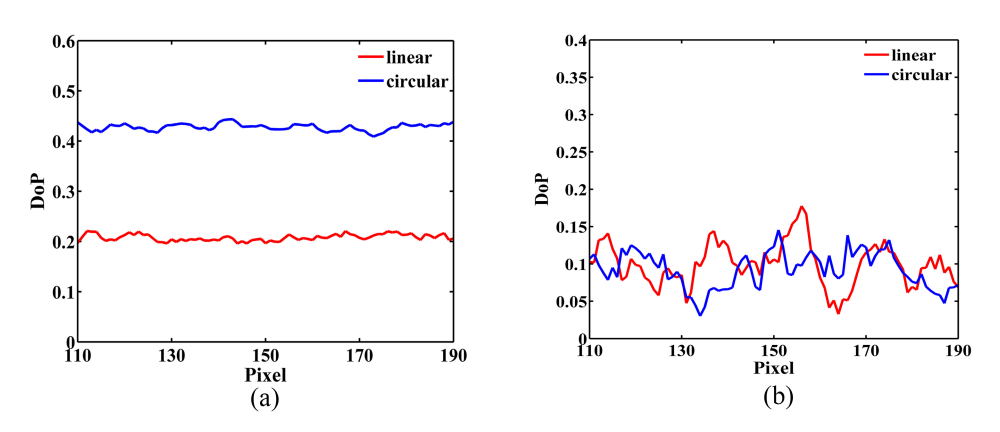


FIG. 9. The spatial distribution of DoP of the backscattered photons without (a) and with (b) the operation of the range-gated technology for the anisotropic medium having a value of $\mu_s = 0.714 \text{ cm}^{-1}$ in the incident photon area for linearly and circularly polarized photons.

The contrast improvement ratios (the difference between the contrast by use of polarizationbased range-gated technology and the contrast by use of intensity imaging divided by the contrast by use of intensity imaging) were also calculated in the scattering media prepared using 0.11 μ m and 2 μ m diameter polystyrene microspheres. By comparing Fig. 10(a) and Fig. 10(b), the extent of contrast improvement is lower in anisotropic scattering medium as compared with isotropic scattering medium for linear and circular PR. To understand this behavior, we recorded the image, denoted as pure image, only formed by the photons that strike the target surface in the propagation process. There is no backscattered photon in the pure image. The intensity profiles of the intensity image, the linear PR image and the pure image along the horizontal direction containing the target center in isotropic and anisotropic media having a value of $\tau = 2.5$ are displayed in Fig. 11. As observed in Fig. 11(a), the intensity profiles of the pure image and the linear PR image have the qualitatively similar distribution while the intensity profile of the intensity image has the highest value. It is the backscattered photons that lead to the deterioration in image contrast in the isotropic medium. Comparing the intensity profiles of the linear PR image and the pure image, it can be observed that linear PR can filter out most of the backscattered photons to improve the image contrast. In contrast to the isotropic medium, for the anisotropic medium, the amount of the backscattered photons decreases and the quantity of the forward-scattered photons increases. The intensity profiles have the qualitatively similar distribution and even the intensity profile of the linear PR image nearly overlaps with the intensity profile of the pure image, as displayed in Fig. 11(b). Not only the backscattered photons but the forwardscattered photons degrade the image quality in the anisotropic medium. The linear PR only can filter out the backscattered photons while the image quality still suffers from the degradation due to the

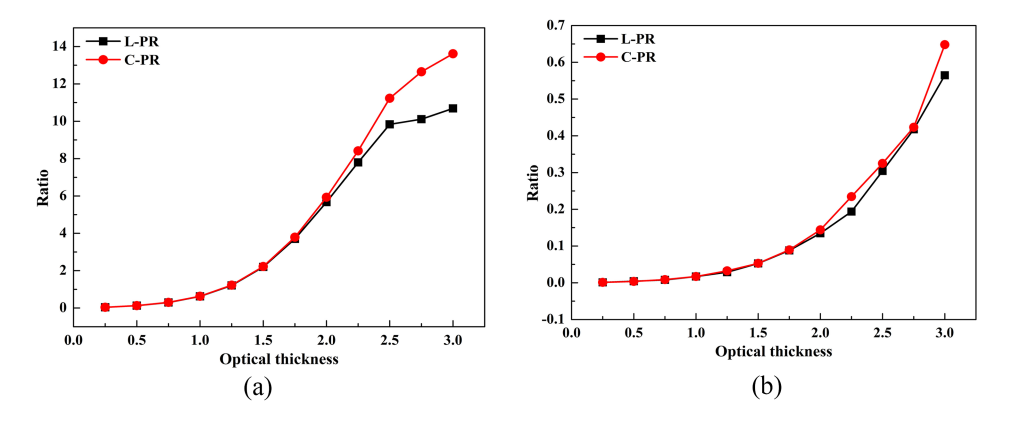


FIG. 10. Variations of contrast improvement ratio with the optical thickness in the medium prepared using 0.11 μ m (a) and 2 μ m (b) diameter polystyrene microspheres. L-PR: the linear PR image and C-PR: the circular PR image.

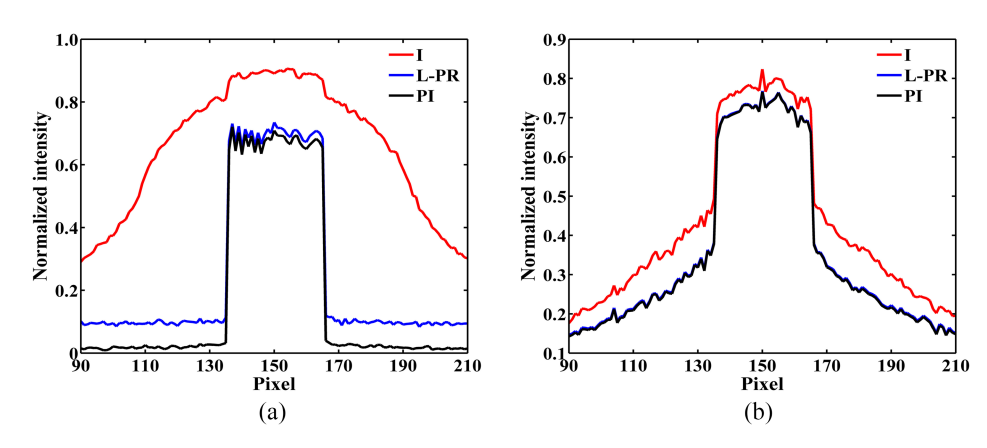


FIG. 11. Comparisons of intensity profiles of the intensity image, the pure image and the PR image for linearly polarized photons in isotropic (a) and anisotropic (b) media having a value of $\tau = 2.5$. It the intensity image, PI: the pure image and L-PR: the linear PR image.

forward-scattered photons. How to utilize the forward-scattered photons to improve the image contrast has also received considerable interest. Similar results were also observed for the case of circular polarization. Therefore, polarization-based range-gated technology can improve the image contrast remarkably in the media composed of large-sized particles by use of the linearly or circularly polarized incident light.

IV. CONCLUSION

In conclusion, a Monte Carlo method for polarization-based range-gated technology was developed to investigate the influence of particle size and the state of polarization of incident light on contrast improvement in turbid media. We extensively investigated the image contrast of the reflective target in scattering media modeled as suspensions of polystyrene microspheres in water with particle diameters of 0.11 μ m and 2 μ m, using linearly and circularly polarized incident light. We have shown that the circular PR is more efficient in improving the image contrast as compared with linear PR for the turbid media composed of small- and large-sized scatterers because of the scattering and depolarization behaviors of polarization light. The effect of particle size on the contrast improvement ratio was also presented. A significant improvement in image contrast has been achieved in isotropic medium using linearly and circularly polarized light due to the dominant influence of forward-scattered photons, resulting in low image contrast in anisotropic medium. These results would be useful for target detection utilizing polarization-based range-gated technology through the turbid media.

ACKNOWLEDGMENTS

Support from China Postdoctoral Science Foundation (2016M592788) is gratefully acknowledged.

¹ J. S. Tyo, M. P. Rowe, E. N. Pugh, Jr., and N. Engheta, "Target detection in optically scattering media by polarization-difference imaging," Applied Optics **35**(11), 1855–1870 (1996).

² S. A. Kartazayeva, X. H. Ni, and R. R. Alfano, "Backscattering target detection in a turbid medium by use of circularly and linearly polarized light," Optics Letters **30**(10), 1168–1170 (2005).

³ Y. Y. Schechner and N. Karpel, "Recovery of underwater visibility and structure by polarization analysis," IEEE Journal of Oceanic Engineering **30**(3), 570–587 (2005).

⁴ H. R. Shao, Y. H. He, W. Li, and H. Ma, "Polarization-degree imaging contrast in turbid media: a quantitative study," Applied Optics 45(18), 4491–4496 (2006).

⁵ Y. L. Gu, C. Carrizo, A. A. Gilerson, P. C. Brady, M. E. Cummings, M. S. Twardowski, J. M. Sullivan, A. I. Ibrahim, and G. W. Kattawar, "Polarimetric imaging and retrieval of target polarization characteristics in underwater environment," Applied Optics 55(3), 626–637 (2016).

⁶ R. H. Wu, J. L. Suo, F. Dai, Y. D. Zhang, and Q. H. Dai, "Scattering robust 3D reconstruction via polarized transient imaging," Optics Letters **41**(17), 3948–3951 (2016).

- ⁷ A. H. Hielscher, J. R. Mourant, and I. J. Bigio, "Influence of particle size and concentration on the diffuse backscattering of polarized light from tissue phantoms and biological cell suspensions," Applied Optics **36**(1), 125–135 (1997).
- ⁸ D. A. Zimnyakov, Y. P. Sinichkin, P. V. Zakharov, and D. N. Agafonov, "Residual polarization of non-coherently backscattered linearly polarized light: the influence of the anisotropy parameter of the scattering medium," Waves in Random Media 11(4), 395–412 (2001).
- ⁹ N. Ghosh, H. S. Patel, and P. K. Gupta, "Depolarization of light in tissue phantoms effect of a distribution in the size of scatterers," Optics Express 11(18), 2198–2205 (2003).
- ¹⁰ X. H. Ni and R. R. Alfano, "Time-resolved backscattering of circularly and linearly polarized light in a turbid medium," Optics Letters 29(23), 2773–2775 (2004).
- ¹¹ R. E. Nothdurft and G. Yao, "Expression of target optical properties in subsurface polarization-gated imaging," Optics Express 13(11), 4185–4195 (2005).
- ¹² R. E. Nothdurft and G. Yao, "Effects of turbid media optical properties on object visibility in subsurface polarization imaging," Applied Optics 45(22), 5532–5541 (2006).
- ¹³ X. X. Guo, M. F. G. Wood, and A. Vitkin, "Monte Carlo study of pathlength distribution of polarized light in turbid media," Optics Express 15(3), 1348–1360 (2007).
- ¹⁴ B. Cochenour, L. Mullen, and J. Muth, "Effect of scattering albedo on attenuation and polarization of light underwater," Optics Letters 35(12), 2088–2090 (2010).
- 15 S. Ghatrehsamani and G. Town, "Propagation of polarized waves through bounded composite materials," Applied Optics 56(4), 952–957 (2017).
- ¹⁶ M. S. Singh, R. Kanhirodan, R. M. Vasu, and D. Roy, "Ultrasound modulation of coherent light in a multiple-scattering medium: Experimental verification of nonzero average phase carried by light," Biomedical Optics Express 3(9), 2100–2110 (2012).
- ¹⁷ J. D. van der Laan, J. B. Wright, D. A. Scrymgeour, S. A. Kemme, and E. L. Dereniak, "Evolution of circular and linear polarization in scattering environments," Optics Express 23(25), 31874–31888 (2015).
- ¹⁸ A. D. Kim and M. Moscoso, "Backscattering of circularly polarized pulses," Optics Letters **27**(18), 1589–1591 (2002).
- ¹⁹ M. Xu and R. R. Alfano, "Circular polarization memory of light," Physical Review E: Statistical Nonlinear and Soft Matter Physics 72(2), 065601 (2005).
- ²⁰ X. X. Guo, M. F. G. Wood, N. Ghosh, and I. A. Vitkin, "Depolarization of light in turbid media: A scattering event resolved Monte Carlo study," Applied Optics 49(2), 153–162 (2010).
- ²¹ J. G. Guan and J. P. Zhu, "Target detection in turbid medium using polarization-based range-gated technology," Optics Express 21(12), 14152–14158 (2013).
- ²² D. Goldstein, *Polarized light, Revised and Expanded* (Marcel Dekker, 2003).
- ²³ L. H. Wang, S. L. Jacques, and L. Q. Zheng, "MCML-Monte Carlo modeling of light transport in multi-layered tissues," Computer Methods and Programs in Biomedicine 47(2), 131–146 (1995).
- ²⁴ C. F. Bohren and D. R. Huffman, Absorption and scattering of light by small particles (Wiley, 1998).
- ²⁵ H. C. van de Hulst, Light Scattering by Small Particles (Dover, 1981).
- ²⁶ N. Ghosh, M. F. G. Wood, and I. A. Vitkin, "Polarimetry in turbid, birefringent, optically active media: A Monte Carlo study of Mueller matrix decomposition in the backscattering geometry," Journal of Applied Physics 105, 102023 (2009).
- ²⁷ Y. Zhang, B. Chen, and D. Li, "Propagation of polarized light in the biological tissue: A numerical study by polarized geometric Monte Carlo method," Applied Optics 55(10), 2681–2691 (2016).
- ²⁸ S. Bartel and A. H. Hielscher, "Monte Carlo simulations of the diffuse backscattering Mueller matrix for highly scattering media," Applied Optics 39(10), 1580–1588 (2000).
- ²⁹ J. C. Ramella-Roman, S. A. Prahl, and S. L. Jacques, "Three Monte Carlo programs of polarized light transport into scattering media: Part I," Optics Express 13(12), 4420–4438 (2005).
- ³⁰ F. Jaillon and H. Saint-Jalmes, "Description and time reduction of a Monte Carlo code to simulate propagation of polarized light through scattering media," Applied Optics 42(16), 3290–3296 (2003).
- 31 W. H. Press, S. A. Teukolsky, W. T. Vetterling, and B. P. Flannery, Numerical Recipes in C: the art of Scientific Computing (Cambridge University Press, 1992).
- ³² D. Côté and I. A. Vitkin, "Robust concentration determination of optically active molecules in turbid media with validated three-dimensional polarization sensitive Monte Carlo calculations," Optics Express 13(1), 148–163 (2005).
- ³³ M. K. Swami, S. Manhas, H. Patel, and P. K. Gupta, "Mueller matrix measurements on absorbing turbid medium," Applied Optics 49(18), 3458–3464 (2010).
- ³⁴ S. Manhas, M. K. Swami, P. Buddhiwant, N. Ghosh, P. K. Gupta, and K. Singh, "Mueller matrix approach for determination of optical rotation in chiral turbid media in backscattering geometry," Optics Express 14(1), 190–202 (2006).
- 35 F. C. MacKintosh, J. X. Zhu, D. J. Pine, and D. A. Weitz, "Polarization memory of multiply scattered light," Physical Review B: Condensed Matter 40(13), 9342–9345 (1989).